LANGMUIR

pubs.acs.org/Langmuir Article

Conformational Changes of Immobilized Polythymine due to External Stressors Studied with Temperature-Controlled Electrochemical Microdevices

Ramya Vishnubhotla,* Christopher B. Montgomery, Kristen L. Steffens, and Steve Semancik

Cite This: *Langmuir* 2021, 37, 2607−2618 Read Online

ACCESS | Metrics & More | Article Recommendations | Supporting Information

ABSTRACT: Conformational changes of single-stranded DNA (ssDNA) play an important role in a DNA strand's ability to bind to target ligands. A variety of factors can influence conformation, including temperature, ionic strength, pH, buffer cation valency, strand length, and sequence. To better understand the effects of these factors on immobilized DNA structures, we employ temperature-controlled electrochemical microsensors to study the effects of salt concentration and temperature variation on the conformation and motion of polythymine (polyT) strands of varying lengths (10, 20, 50 nucleotides). PolyT strands were tethered to a gold working electrode at the proximal end through a thiol linker via covalent bonding between the Au electrode and sulfur link, which can tend to decompose between a temperature range of 60 and 90 °C. The strands were also modified with an electrochemically active methylene blue (MB) moiety at the distal end. Electron transfer (eT) was measured by square wave voltammetry (SWV) and used to infer information pertaining to the average distance between the MB and the working electrode. We observe changes in DNA flexibility due to varying ionic strength, while the effects of increased DNA thermal motion are tracked for elevated temperatures. This work elucidates the behavior of ssDNA in the presence of a phosphate-buffered saline at NaCl concentrations ranging from 20 to 1000 mmol/L through a temperature range of 10−50 °C in 1° increments, well below the decomposition temperature range. The results lay the groundwork for studies on more complex DNA strands in conjunction with different chemical and physical conditions.

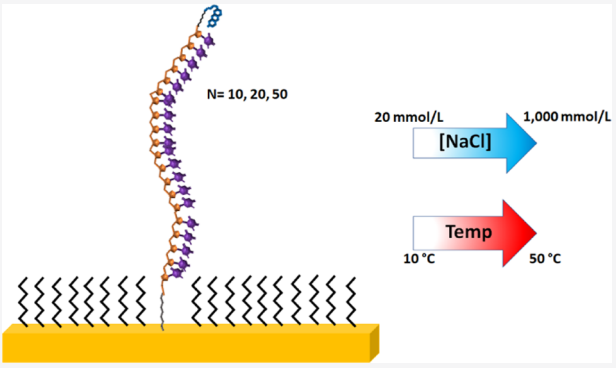

INTRODUCTION

Biosensing is a critical field of research that can impact a range of medical areas from drug discovery to clinical diagnostics. As one example, the need for point-of-care technology and rapid sensor-based screening tools has certainly been made exceedingly clear by the recent H5N1 and COVID-19 pandemics. Associated with this demand for widely deployable and inexpensive devices is the stringent requirement that detection of the target biomarker be highly reliable. Therefore, biomolecular interactions between the biomarker and sensor and related processes involved in producing a signal must be consistent and well understood.

Sensing interfaces involve an assortment of biomolecules, with nucleic acids being one of the most popular, either as the biomarker itself or as a biorecognition element.[1−6] While RNA and PNA formats are becoming increasingly important,[7−9] the most common form of nucleic acid studied is DNA, immobilized either in the single-strand or double-strand form, with one of the earliest examples being the work of Palacek, who studied the melting profiles of dsDNA and their effects below melting, or denaturation, temperature.[10] Often, DNA strands are modified with tags that assist in transducing the signal, as is typically the case in electrochemical (EC) sensing[11−13] and fluorescence detection.[14,15] Apart from these methods, DNA may also be used in label-free biosensing through surface-enhanced Raman spectroscopy (SERS)[16] and surface plasmon resonance (SPR).[17] DNA biosensor studies have been conducted and are crucial for developing cost-effective, time-efficient, and simpler approaches for sensing that can be used in place of more expensive detection methods such as liquid/gas chromatography-mass spectrometry (LC-MS/GC-MS) or in conjunction with more affordable and effective technologies such as polymerase chain reaction (PCR).[1,18]

Electrochemical (EC) sensors, which transduce a chemical reaction into an electrical signal, have been used for studies of ligand binding with double-stranded DNA,[19] DNA hybrid-

Received: November 6, 2020
Revised: January 27, 2021
Published: February 17, 2021

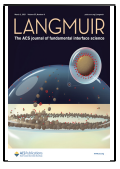

https://dx.doi.org/10.1021/acs.langmuir.0c03219
Langmuir 2021, 37, 2607−2618

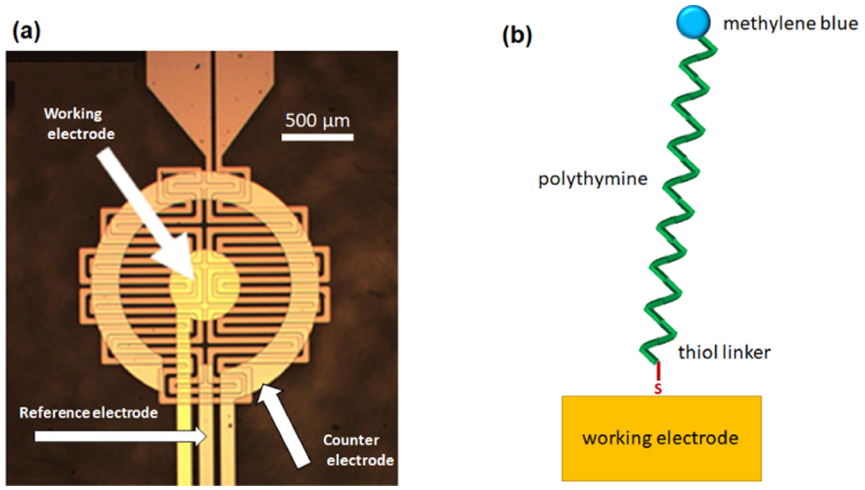

Figure 1. (a) Microscope image of an electrochemical device as seen from above, with an embedded Pt serpentine PRT insulated from a Pt counter electrode (CE), Pt quasi-reference electrode (RE), and a central Au working electrode (WE); (b) cross-sectional schematic of a DNA polyT strand bound to the gold working electrode of the device through thiol-linking and including a methylene blue moiety at the distal end.

ization through conducting polymer sensors,[20] single-nucleotide polymorphism (SNP) detection,[21] protein detection,[22,23] and drug sensing.[24] EC sensors may also be used to detect biomolecules through the incorporation of aptamers, which are short-stranded nucleic acid sequences that change conformation upon binding with a target analyte.[25,26] Aptamers can be ideal probes for sensing, as they can be selected to specifically bind a wide variety of biomolecules, ranging from market drugs[6] to peptides[27] and proteins.[28]

Whether one employs duplex DNA or more complex DNA structures such as aptamers for EC sensing, monitoring is likely performed in a range of environments. Differences in pH, buffer chemistry, ionic strength, and temperature can cause conformational changes (secondary or tertiary structure) as well as folding that may inhibit the binding interactions for which they were intended in a sensor assembly.[24] Therefore, understanding how environmental factors alter the orientation and geometry of immobilized biomolecules and how those changes might affect the general sensing signals is important. In an effort to directly correlate measured electrochemical signals with the action of environmental stressors, we conducted studies of simple polythymine (polyT) strands immobilized on gold electrodes. Differing lengths were examined and all polyT samples were synthesized with an electrochemically active methylene blue (MB) moiety at the distal (3′) end, and a disulfide group used at the proximal (5′) end to bind to the Au device electrode. The polyT strand can be considered as a model nucleotide strand and a special/simplistic form of an aptamer due to the minimal base-pair or stacking interactions.[29] We investigated measured current variations associated with differing strand length and conformational changes induced in the tethered polyT as a result of external stressors, specifically, variations in the chemical environment (i.e., NaCl concentration) and temperature change.

MB-tagged DNA has been used extensively for biosensing, in tracking hybridization,[19,30] DNA mismatches,[21] binding events,[31] and measuring increases or decreases in signal as a function of temperature, with or without DNA labels.[32−36] Doose et al. have employed fluorescence correlation spectroscopy to investigate diffusional translation in salt solutions, with varying salt concentrations.[37] Silva et al. have studied similar systems, with two different redox tags on a DNA strand, reporting that there can be effects of ion screening that hinder the signal coming from having the moiety closer to the electrode.[38] Uzawa et al. have studied the mechanisms of electron transfer from MB redox tags for immobilized polyT samples to examine how the flexibility of the strand changes with the salt concentration of its buffer, by studying the distance between the MB redox tag and the Au electrode of an electrochemical device, as well as the persistence length of the polyT strand.[39] The reported current was referred to as the equilibrium current, in that the electron transfer is determined by equilibrium statistics rather than chain dynamics. In this study, we refer to the "average current" as the current measured at the average position of the moiety with respect to the electrode.

Here, we report on the effects of temperature and salt concentration on the morphology of polyT strands of varied length (10, 20, and 50 nucleotides, referred to from this point on as 10-mer, 20-mer, and 50-mer, respectively). The morphological changes were monitored by measuring the oxidation/reduction currents from a MB tag attached to the strands, which were tethered to a gold electrode. The effects of temperature range and varying salt concentrations of the working buffer were studied for each strand length, thus allowing for qualitative comparison between strands and ionic strength (NaCl concentration). We found that a temperature increase appears to cause stretching in the 10-mer polyT, and that elevated temperatures can cause stretching of the 10-mer and 20-mer polyT strands at high salt concentrations. For lower salt concentrations of the 20-mer and 50-mer strands, we observe the effects of what we believe is salt-induced flexibility combined with thermal motion of the strand, which have both been found to be more prominent for ssDNA than for hybridized DNA strands.[40] While the salt concentration of the environment affects the rigidity of the strand, different length strands exhibit somewhat unique electrochemical signatures when exposed to these stressors. These model studies provide insight into the nature of the current-based signals and temperature-dependent profiles as stressor-induced ssDNA conformation changes. With this knowledge, we are better poised to move forward with more complex studies on DNA-based aptamers en route to the development of reliable sensors

https://dx.doi.org/10.1021/acs.langmuir.0c03219
Langmuir 2021, 37, 2607−2618

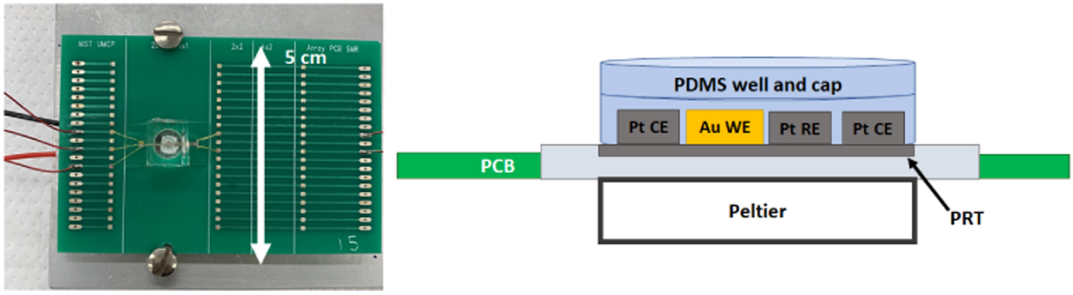

Figure 2. Top image (left) and side schematic (right) of the device mounted with epoxy on a PCB and a Peltier unit underneath to heat/cool the EC sensing interface. A poly(dimethylsiloxane) (PDMS) well and cover on top of the device is used to contain the sample and prevent evaporation. The drawing on the right (not to scale) shows a representative schematic of the device configuration.

for the application in medical diagnostics or therapeutic drug monitoring.

EXPERIMENTAL SECTION

Materials. The electrochemical platforms (see below) were fabricated in-house and are reusable, temperature-controlled microdevices that facilitate rather rapid electrochemical analyses of small-volume samples (<10 μL). The polyT strands were purchased from Integrated DNA Technologies* (Coralville, IA) and Biosearch Technologies* (Novato, CA) with dual HPLC purification and were used as received. Tris base, ethylenediaminetetraacetic acid (EDTA), sodium phosphate monobasic, sodium phosphate dibasic, sodium chloride, tris 2(2-carboxyethyl) phosphine hydrochloride (TCEP), and 6-mercapothexanol were purchased from Sigma Aldrich* (St. Louis, MO) and used as received. Chemical reagents were all of analytical grade or higher. Deionized ultrafiltered (DIUF) water had the desired resistance of 18.2 MΩ·cm.

The DNA was reconstituted to 100 μmol/L concentration in a Tris/EDTA (TE) buffer (10 mmol/L Tris base, 1 mmol/L EDTA, and buffered to a pH of 8.0 using NaOH and HCl). Phosphate-buffered saline (PBS) solutions were prepared with 5 mmol/L sodium phosphate monobasic, 5 mmol/L sodium phosphate dibasic, and the respective NaCl concentration (20 mmol/L to 1000 mmol/L) and buffered to a pH of 7.4 with NaOH. All solutions were prepared using >18 MΩ deionized ultrafilter (DIUF) water.

Platform Assembly. Planar electrochemical microdevices were fabricated in-house at the NIST Center for Nanoscale Science and Technology NanoFab Facility and were reported on in a previous study.[19] In brief, multiple individual sensors, like that shown in Figure 1a, were created on a 4 in. fused-silica wafer. Each has an embedded Pt serpentine structure which functions as a platinum resistance thermometer (PRT) and has also been used as an integrated resistive microheater in other studies.[41] A SiO_2 insulation layer of thickness 1 μm and electrodes of Pt and Au were located over the PRT, as reported previously.[19] The electrodes included an Au working electrode (WE), where the polyT is immobilized (Figure 1b), a Pt quasi-reference electrode (RE), which establishes an electrical potential against which all other potentials are measured, and a Pt counter electrode (CE), which is used in conjunction with the WE to achieve current flow. The sensors were attached to a small printed-circuit board (PCB) to provide easy accessibility and a reliable connection to electronics. A commercial Peltier device* (MS2-010-06-06-11-11-00-W2, Laird Technologies Inc., Chesterfield, MO) was also mounted on the PCB beneath the sensor for cooling and heating (see Figure 2). Before beginning sensing experiments, the devices were thermally calibrated in an oven to account for slight device-to-device differences in resistance of the PRT. To calibrate the microdevices, current values as a function of temperature from 20 to 80 °C, in increments of 10 °C, were recorded for a constant applied voltage of 0.5 V. The resulting calibration for each device was used in conjunction with the EC sensing control program during data collection to specifically account for the resistance of each individual sensor and approximate the temperature of the device.

Preparation of Immobilized Polythymine. The polyT DNA was purchased premodified at the proximal end (5′) with a sulfide group to bind to the Au working electrode of the EC sensors through thiol-linking, with a methylene blue (MB) redox reporter at the distal end (3′). The MB reporter was included to provide a viable means of signal tracking for the effects of temperature and chemical environment variation on the polyT conformation.

To prepare the DNA for experimentation, 1 μL of the 100 μmol/L DNA solution was mixed with 2 μL of 20 mmol/L TCEP solution in DIUF water. The purpose of the TCEP was to cleave the disulfide bond in the purchased DNA, to ensure proper thiol binding to the Au electrode. The solution was left to incubate in a high humidity environment at room temperature for 90 min. During this incubation step, the devices used were cleaned, first with a Piranha solution of 3 parts by volume H_2SO_4 and 1 part H_2O_2 (*Caution*: Piranha solution is highly exothermic, and it is imperative that the H_2O_2 be added to the H_2SO_4; it is also highly explosive and should not come into contact with organic materials.) in which it was incubated for 2 min, and then the device was rinsed with DIUF water and dried with pressurized N_2. Next, an electrochemical cleaning was performed to help further remove organic material from the electrode surface. The CV scan window was −0.9 to 0 V versus the Pt pseudoreference electrode, with a scan rate of 0.1 V/s for 20 cycles in 20 μL of a 0.5 mol/L H_2SO_4 solution. The device was then rinsed with DIUF water and dried with pressurized N_2. Following the TCEP reduction step, a NaCl (250 mmol/L) phosphate-buffered saline (PBS, pH 7.4) was added to the TCEP/DNA solution to dilute the DNA concentration to 50 nmol/L. This concentration proved to be high enough to achieve an immobilized layer with a low-noise electrochemical signal while potentially precluding steric interactions between the immobilized DNA strands. Figure S1 in the supplemental section shows that the 50 nmol/L concentration is apparently far from the surface saturation limit, as determined through measurements of the nitrogen (N 1s) feature measured by X-ray photoelectron spectroscopy (XPS). These characterizations were performed on separate Au-coated substrate samples exposed to varying DNA concentrations of a 20-mer polyT strand. For all experiments (10-mer, 20-mer, 50-mer), 10 μL of the 50 nmol/L DNA solution was pipetted onto the device and left to incubate for 1 h after which the device was gently rinsed with DIUF water and dried with N_2. Next, 10 μL of 2 mmol/L 6-mercaptohexanol in 250 mmol/L NaCl PBS was pipetted onto the device and left to incubate in the dark for 1 h, to prepare a self-assembled monolayer (SAM). The SAM layer served the purpose of reducing nonspecific adsorption of the DNA to the Au working electrodes. Following this last surface functionalization step, the SAM solution was rinsed with DIUF water, and the device was dried with pressurized N_2 one final time before use.

Data Collection. Each mounted EC microdevice was connected to a power source (E36313A Keysight Technologies*, Santa Rosa, CA) and a source measure unit (SMU) (B2902A Keysight Technologies*, Santa Rosa, CA) for sweeping the applied voltage during data collection. Measurements were conducted with an electrochemical workstation (CHI1040c, CH Instrument Inc.*, Austin, TX). The experimental control interface (see also the

https://dx.doi.org/10.1021/acs.langmuir.0c03219
Langmuir 2021, 37, 2607−2618

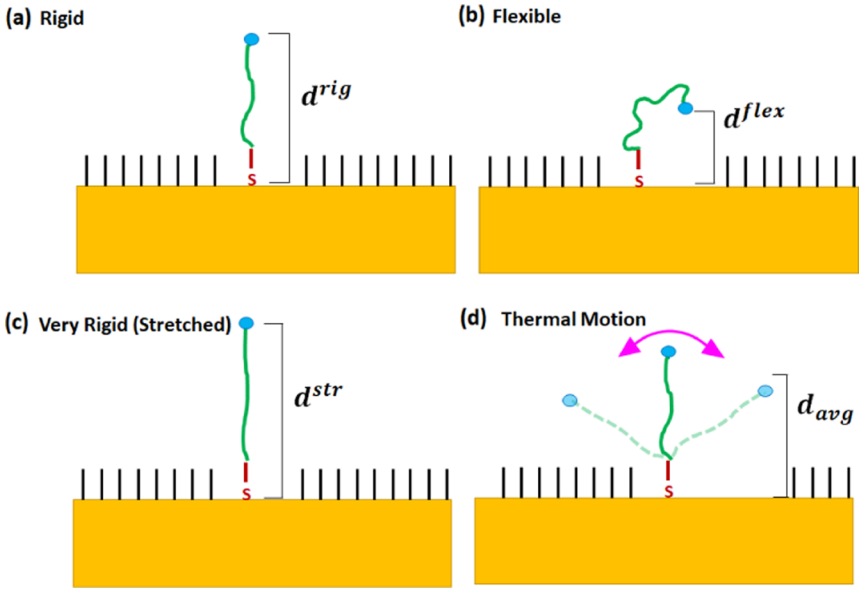

Figure 3. Factors affecting the measured current level (a) rigidity of the strand, wherein the moiety is far from the Au electrode, represented as d^{rig}; (b) minimal rigidity/maximum flexibility of the strand, bringing the moiety closer to Au, and represented as d^{flex}; (c) stretching of the strand (high rigidity), moving the MB farther away, represented as d^{str}; (d) thermal motion of the strand, shown here as bringing the average position for the MB closer to the Au in multiple directions, represented as d_{avg}; The current in all cases is influenced by $1/d$, where d is the distance between the moiety and the Au electrode. We suggest that the profile for a strand's flexibility due to ionic concentration can range from rigid to moderately flexible, to overcharged, the last of which is extremely rigid. The profile for a strand's thermal motion due to heating can range from minimal motion to moderate motion, to stretching, the last of which also results in minimal motion.

Supporting Information—Electrochemical Control Program and Data Collection Methods) utilized the embedded PRT of the device to monitor the temperature varied by the commercially purchased Peltier unit located underneath the electrodes, which was employed to heat/cool the working buffer solution, and is an improvement on the program used in a previous study, which had manual voltage set points.[15] A PDMS well with a 2.5 mm diameter hole was placed atop the devices to contain the working buffer solution necessary for liquid sample sensing, and it was covered with a PDMS cap to prevent evaporation of the small-volume solution (Figure 3).

Conformational changes in polyT strands were examined via electrochemical measurements as a function of ionic strength ([NaCl]) and temperature using our microscale electrochemical platform. Electrochemical response was determined through square wave voltammetry (SWV) and the peak currents were measured (near −0.5 V) for each temperature set-point. Electrochemical signals were a result of the two-electron transfer between the MB redox tag and the Au electrode, influenced by the proximity of the MB to the Au. Salt concentrations were used sequentially beginning at the lowest salt during a ramp up, after which the temperature was held for 2 min to allow for removal of the "old" solution and addition of the "new solution" of the next highest ionic concentrations, stepped down in temperature and held again for 2 min, at which point the next highest salt solution was used (see Figure S2, which presents a comparison of results from this alternating ramp-up/ramp-down data acquisition method with an earlier approach). The temperature steps were between 10 and 50 °C in 1° increments every 25 s, at a frequency of 60 Hz, a sensitivity of 1 μA to obtain thermal profiles and a voltage range sweep of −0.7 to −0.2 V with an amplitude of 0.025 V, and a step size of 0.001 V for a 20-mer. In this setup, the working electrode is at open-cell potential when the voltammogram is not being acquired.

The packing densities of the DNA strands on the electrode surface were estimated to be between 1×10^{12} and 1×10^{13} molecules/cm^2. The density calculations were based on the current obtained during CV sweeps, converted to overall charge (coulombs) based on the frequency used in the program (60 Hz), divided by the approximate geometric area of the WE, 0.003 cm^2.[19] Final estimates of the number of molecules per unit area are based on the charge of each DNA strand (where each MB has an exchange of two electrons with the Au per strand). These packing densities are comparable to previous reports of packing densities on the order of 1×10^{12} molecules/cm^2, which yield a separation of around 10 nm between probes,[42,43] and packing densities of between 1×10^{12} and 11×10^{12} DNA strands/cm^2 as measured through CV for DNA with a MB tag.[44] Consequently, we assume in this study, consistent with the XPS measurements in Figure S1, that steric effects between neighboring DNA probes are likely to be small or negligible and that DNA aggregation is at a minimum,[45,46] as the concentration used is well below the maximum coverage concentration while still being large enough to yield a notable signal. Finally, Rashid et al. found that the thiol-linking between a DNA strand and a Au electrode are strong enough to prevent desorption of the DNA, and therefore, we do not anticipate any effects of DNA desorption in this study.[47]

RESULTS AND DISCUSSION

Sources of Current. As indicated, this study used a planar microscale electrochemical platform to measure current from polyT strands that were thiol-tethered to the Au working electrode at the 5′ end and have methylene blue (MB) redox tags attached at their distal ends (3′ end). MB redox reactions provide features that can be tracked by measuring current levels, which depends on MB proximity to the Au electrode, over a potential range in small increments over time, and are therefore a common choice for an electrochemical sensing approach. Some biosensors are termed "off-on" sensors[48−50] when they go from producing essentially no current, as in the case when MB is far from the WE where electrochemical transfer cannot occur, to producing a measurable current when the MB moiety is sufficiently closer to the WE to allow measurable electron transfer. In a previous study, Silva et al. found that the positioning of the MB redox tag on ssDNA plays a role in the measured current transfer. It was found that a MB tag at the proximal end of the DNA strand actually produced a considerably smaller signal than one at the distal

https://dx.doi.org/10.1021/acs.langmuir.0c03219
Langmuir 2021, 37, 2607−2618

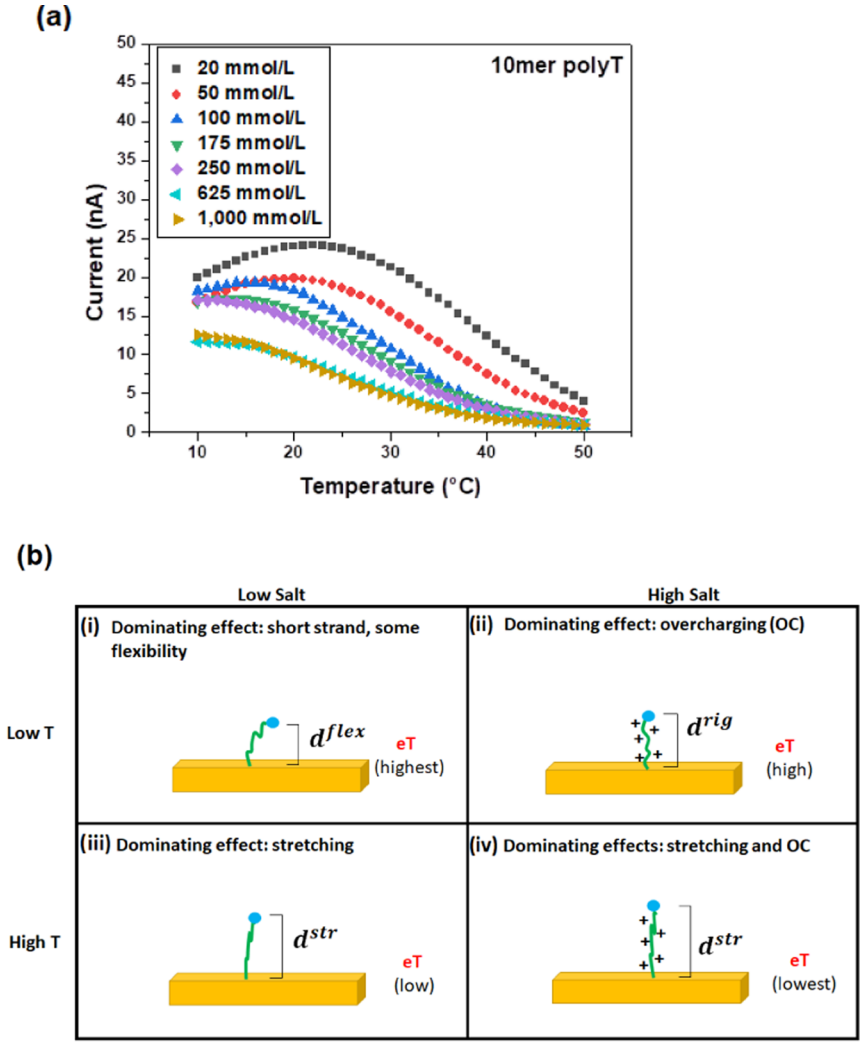

Figure 4. (a) Peak current versus temperature profile of a single run of 10-mer polyT in varying salt concentrations; (b) schematics of effects that may explain the behavior of 10-mers as a function of both temperature and ion concentration. The electron transfer (eT) level descriptors (low to high) give qualitative comparative magnitudes for the measurements of this strand under different conditions.

end, due to counterion accessibility. In that same study, it was stated that a farther or distal MB tag allowed for faster transfer kinetics.[38] In a separate study by Silva et al., a MB was also tested at points in the middle of the DNA strand, showing a progression of increasing current as the MB redox slowly approaches the distal end.[51] This study uses the simplest case, where the MB tag is at the distal end, precluding counterion effects reported by Silva.

On the other hand, sensors can continually monitor changes in current such as with graphene biosensors, where a voltage of zero still yields some current due to graphene's lack of a band gap.[52−54] In cases with simple immobilized nucleotide strands (e.g., polyT), the current-producing process at a particular voltage in the electrochemical cell can be controlled almost entirely by the distance between the MB and the WE. This process was demonstrated by Uzawa et al., wherein the electron transfer rate between a MB tag and a WE was measured for a polyT strand, and the effects of persistence length and chain flexibility were studied.[30] In the case of polyT in those studies, a negligible current appeared to be transported through the DNA strand, due to the high redox potential of polyT.[39,55] Additionally, a study by Pheeney and Barton reported electron transfer for both ssDNA and dsDNA with a MB tag and found that ssDNA itself does not efficiently conduct charge and has a high affinity for a Au surface.[56] Because of the more complex aspects of the study reported here with both varying ionic strength and temperature, other contributions to the measured current must also be examined.

The average distance between the MB and WE is a major factor in the measured current in this system. In addition to the length of the polyT chain, the average distance depends on the rigidity and conformation of the polyT, both of which depend upon [NaCl] and temperature. One can also consider whether the redox behavior of the MB tag itself is in any way influenced in a solution where either temperature, the [NaCl], or both are changing.

SWV is commonly used in electrochemical biosensing. It utilizes a staircase potential gradient that, at each step, applies a "reverse" pulse with potential slightly below the potential step and a "forward" pulse with potential slightly above the potential step; this sequence is equivalent to a square wave function added to the staircase function. The difference of the currents measured between the forward and reverse pulses, known as the differential current, allows for the removal of non-Faradaic currents resulting from charging effects rather than electron transfer.[57,58] The measurement procedure

https://dx.doi.org/10.1021/acs.langmuir.0c03219
Langmuir 2021, 37, 2607−2618

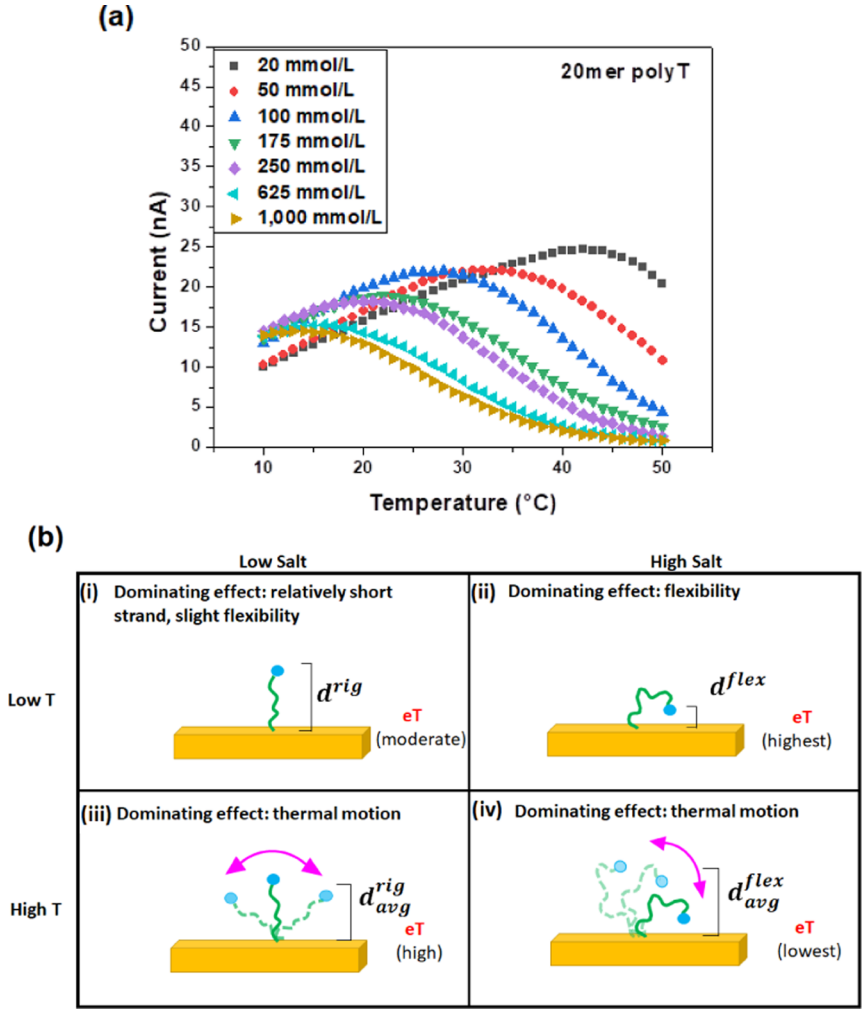

Figure 5. (a) Peak current versus temperature profile of a single run of 20-mer polyT in varying salt concentrations; (b) schematics of effects that may explain the behavior of 20-mers as a function of both temperature and ion concentration. The electron transfer (eT) level descriptors (low, moderate, high) give qualitative comparative magnitudes for the measurements of this strand under different conditions.

involves scanning a potential window to find a maximum differential current value, referred to as the SWV peak current. According to Meunier-Prest et al., SAM layers are electroactive within a potential range of +0.8 to −1.4 V versus saturated calomel electrodes (SCE). In this potential range, SAM layers are expected to retain their structural order and high packing density, especially in an aqueous medium.[59] In our experiments, the SWV window was approximately −0.7 to −0.2 V, well within the electroactive range with the peak generally appearing around −0.45 V, regardless of strand length, with minimal variations (less than 10%) (see Figure S3). Because we do not observe large variations in the peak voltage, we do not expect this voltage to have an effect on the conformation, and therefore the current, of the polyT. Kaiser et al. have discovered a relationship between voltage and current for single-strand DNA, especially in the case of increased temperature.[60] Studies have also shown the effects of the electric field in being able to dehybridize dsDNA,[61] and that modulation of both ssDNA and dsDNA is observed due to changing frequencies, as well as responsiveness to electrostatic perturbations.[62] However, our study only employs a frequency of 60 Hz.

Varying the salt concentration and the temperature affects the flexibility and motion of the strands, which in turn affect the measured current, and we note that both salt concentration and temperature can either increase or decrease the current levels. This behavior can be seen in Figure 3, which demonstrates discrete (but in some cases related) phenomena that we hypothesize can alter the distance between the MB and Au WE. In the figure, d^{flex}, d^{rig}, and d^{str} are parameters that represent various effects controlling the MB−WE distance. Figure 3 specifically treats these discrete phenomena, which can be looked at as part of a continuum that ranges from very flexible toward rigid and stretched. Furthermore, d_{avg} is the average MB−WE distance and is based on the induced thermal motion of the strand, which occurs whether the strand is rigid, flexible, or stretched. Generally, the more flexible an oligomer is, the more pronounced the random thermal motion will be. For a very rigid strand, the thermal motion will be constrained to rotation around the anchoring pivot point.[63] This behavior was also previously reported in a study by Anne and Demaille, which demonstrated that free hinge motion due to thermal agitation about the anchoring point of a tethered DNA strand could augment or decrease the current signal from the moiety.[64] Additionally, the charge of the electrode, here, negative of the point-of-zero charge (pzc), during the experiment will have some effect on the polyT strand's ability

https://dx.doi.org/10.1021/acs.langmuir.0c03219
Langmuir 2021, 37, 2607−2618

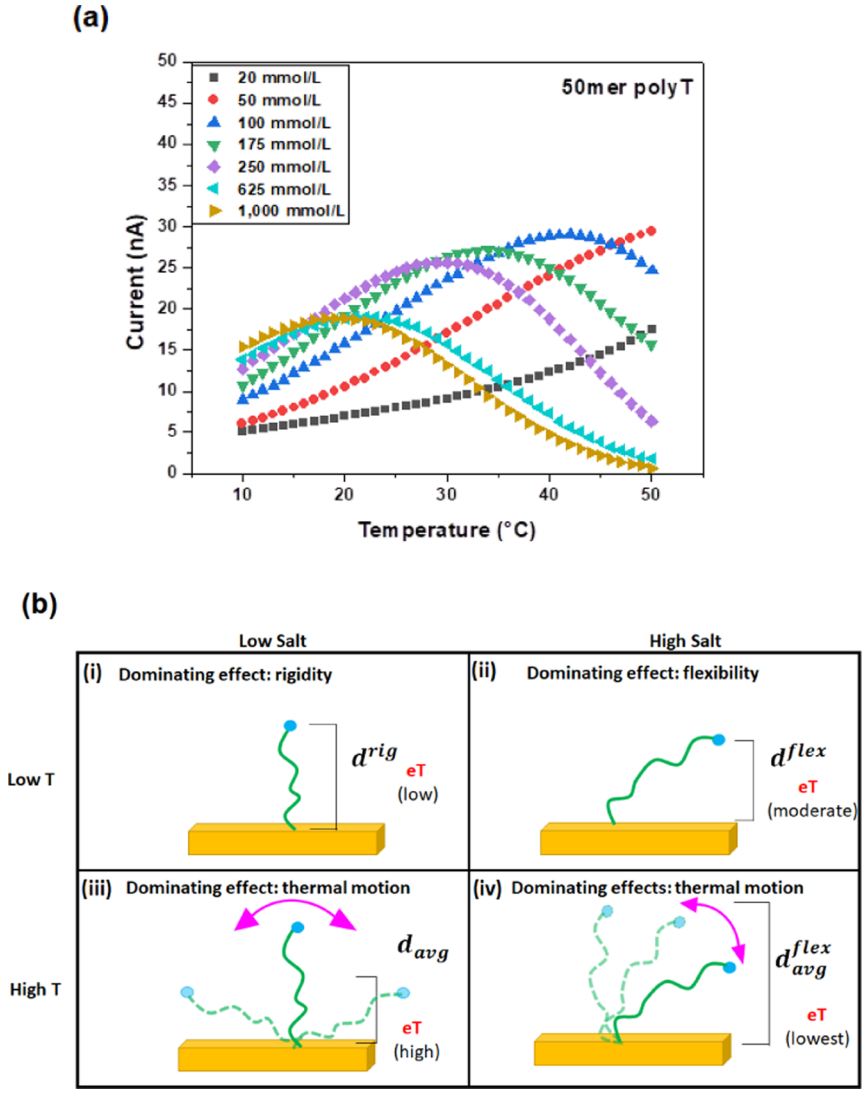

Figure 6. (a) Peak current versus temperature profile of a single run of 50-mer polyT in varying salt concentrations; (b) schematics of effects that may explain the behavior of 50-mers as a function of both temperature and ion concentration. The electron transfer (eT) level descriptors (low, moderate, high) give qualitative comparative magnitudes for the measurements of this strand under different conditions.

to approach the Au in low salt environments due to charge repulsion between the electrons and the electrode.[65]

The effects of temperature and salt concentration variations are not necessarily the same for different polyT strand lengths. Additionally, a single effect can dominate another when combining these two stimuli, and therefore, we must address each polyT strand case separately. For EC measurements on each of the strand lengths, the temperature range was set from 10 to 50 °C, measuring the SWV current at 1° increments. This temperature range was swept for each of seven different salt concentrations, from 20 to 1000 mmol/L. The experimental solutions were composed of 10 mmol/L phosphate buffered with varying levels of NaCl and buffered to a pH of 7.4. Each set of tests was completed three times. Figure S4 indicates the reversibility of this data collection method, and Figure S5 shows the reproducibility of the method.

10-mer PolyT. Data for the polyT 10-mer current versus temperature are shown in Figure 4a for the seven salt concentrations studied. The schematics in Figure 4b show conceptually how the phenomena in Figure 3 may explain the ways that temperature and salt concentration affect the eT, and therefore the measured current.

Although influenced by changing temperature and salt concentration, the 10-mer exhibited a generally similar thermal profile for all of the salt concentrations. At low temperature, where the currents for this short strand are somewhat higher than those corresponding currents for the longer 20-mer and 50-mer, and low salt concentration, we see a high current, mostly likely due to some flexibility and relative proximity of the MB to the Au. As temperature and salt concentration increase, we see a decrease in the signal, which we believe to be a combination of overcharging and stretching, where the stretching is the most energetically favorable phenomenon for an overcharged, positive strand. According to a study by Belkin et al., single-strand DNA threaded through a nanopore exhibited an increase in the length of the chain in response to temperature increase and gradient, referred to as "stretching".[66] Interestingly, Kaiser et al. also noticed a stretched state for ssDNA under increased temperature and especially for fixed negative potentials.[60] Although our setup involves sweeping a potential range, and not a fixed potential,

https://dx.doi.org/10.1021/acs.langmuir.0c03219
Langmuir 2021, 37, 2607−2618

we believe we are still observing ssDNA in a stretched state due to temperature increases.

It is well known that higher salt concentrations can neutralize the negatively charged phosphate backbone of the DNA, allowing it to become more flexible in its conformation.[67,68] We believe that low salt concentration is enough to slightly increase the flexibility of the 10-mer strand, which has relatively low charge due to a small number of nucleotides, but we ascribe the decrease in current as salt concentration increases to the excess charge of cations in the working buffer solution "overcharging" the DNA strand, also known as charge reversal, which has been hypothesized through simulation studies.[69,70] We speculate that this charge reversal happens only when the amount of salt is relatively high such that there are enough ions to overcharge the strand. In this charge reversal, we expect the negatively charged DNA to no longer be neutral due to the salt in the buffer, but to now be positively charged due to an excess of cations. This makes the now-positively charged strand increase in rigidity, due to the repulsion of the now positive−positive charges along the DNA backbone. In this case, the MB moiety would be farther away from the Au than for a moderate salt concentration, decreasing eT.

Additionally, an overcharged strand may be more prone to stretching than a neutral and flexible strand, which appears to be in agreement with prior observations. For example, Wenner et al. discovered that overstretching with optical tweezers in double-strand DNA was more favorable in high salt concentrations than low salt concentrations.[71] It is possible that overcharged strands, which are positively charged from excess salt, are more prone to stretching, as this is the most energetically favorable conformation due to the repulsion of like charges along the DNA contour.

20-mer PolyT. Data for the polyT 20-mer current versus temperature are shown in Figure 5a for the seven salt concentrations studied. The schematics in Figure 5b show conceptually how the phenomena in Figure 3 may explain the ways that temperature and salt concentration affect the eT, and therefore the measured current.

For a 20-mer polyT strand, we observe some decrease of current as a function of temperature in higher salt solutions, but observe an increase in current as a function of temperature in the two lowest salt solutions. Essentially, the behavior of a 20-mer strand seems to have regimes of different behavior at low salt concentrations and high salt concentrations, transitioning gradually from one to another. At low salt, when the strand is only slightly flexible, we see an increase in the current with temperature, attributed to thermal motion bringing the MB closer to the WE. For higher salt concentrations and high temperatures, we believe that thermal motion is still the dominating effect, except in this instance; the strand begins in a flexible instead of a rigid state, therefore allowing the MB to move farther away from the WE and thereby decreasing the measured current. It is interesting to note that the effects of thermal motion on current are dependent on the initial flexibility of the strand.

50-mer PolyT. Finally, data for the polyT 50-mer current versus temperature are shown in Figure 6a for the seven salt concentrations studied. The schematics in Figure 6b show conceptually how the phenomena in Figure 3 may explain the ways that temperature and salt concentration affect the eT, and therefore the measured current.

We suspect that the 50-mer polyT strands are not as prone to being overcharged by the salt solutions used in this study, due to the greater amount of charge on a longer strand, which would require considerably more ions to cause overcharging compared to a 10-mer polyT strand. However, flexibility can be expected to increase and contribute to increased current in response to greater salt concentrations. We do note an increase in the current as of the temperature increases for low salt concentrations, and therefore, it seems likely that no observable effects of stretching appear for a 50-mer polyT strand in this temperature range. A previous study showed stretching for a 54-mer ssDNA in the presence of a solution adjacent to a 95 °C heater;[66] however, our experimental sample and setup are different. Instead, our 50-mer data shows an increase in current probably dominated by increased flexibility, combined with heat, which creates thermal motion and further augments the signal. The 50-mer results looked similar to the 20-mer, indicating that perhaps some polyT "length limit" exists after which the behavior begins to look consistent for each salt concentration and temperature.

One notable trend from the data shown in Figures 4−6 is how the effects of stretching diminish as the strand moves away from being "overcharged" and becomes more neutral. This trend suggests a positive correlation between overcharging (or very high salt concentrations) and stretching, most likely due to the electrostatic effects of the now-positively charged polyT strand, where the stretched state is the most energetically favorable.

To further assess our presented concepts for the behavior of the 10-mer, 20-mer, and 50-mer, we can turn to trends derived from the data of Figures 4−6. Figure 7 shows the temperature at which the maximum current occurs as a function of salt concentration. We observe the same trend for all three-strand

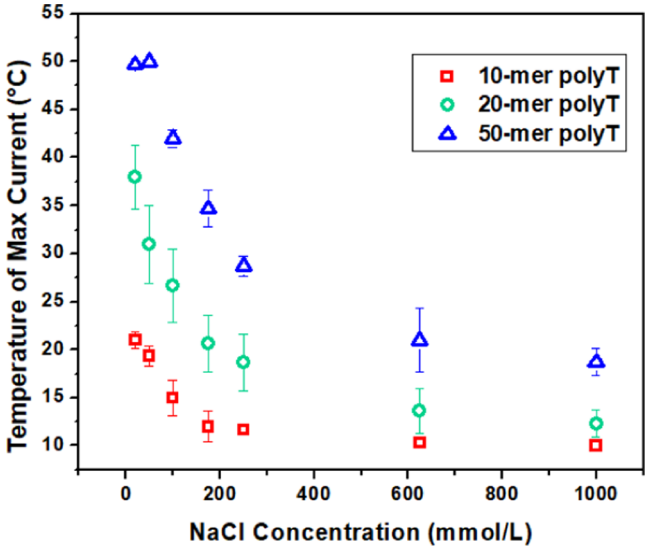

Figure 7. Trends for the temperature of maximum observed current (within the studied range of 10−50 °C) versus salt concentration for 10-mer polyT (red squares), 20-mer polyT (green circles), and 50-mer polyT (blue triangles). The plots shown here were obtained using data from three separate trial runs (beginning with Piranha and CV cleaning, followed by DNA attachment, and SAM attachment) at each salt concentration and for each strand length and show an increase in temperature of maximum current as the strand length increases. Error bars are the standard error of the mean for a population with a 95% confidence interval.

https://dx.doi.org/10.1021/acs.langmuir.0c03219
Langmuir 2021, 37, 2607−2618

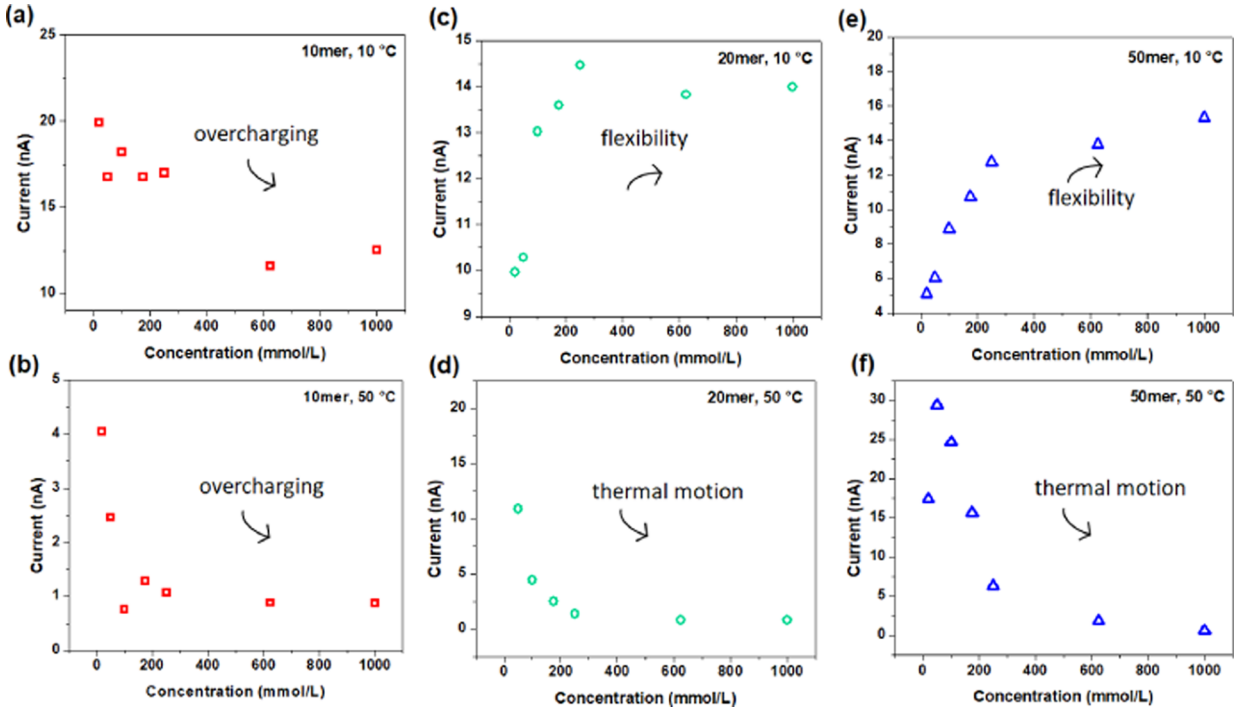

Figure 8. Peak current versus NaCl concentration for all three polyT strand lengths (left, middle, and right) plotted for fixed temperatures, taken from the data in Figures 4–6. In each case, the hypothesized effect that dominates the observed trend is indicated: (a) 10-mer at 10 °C, dominated by overcharging from excess cations; (b) 10-mer at 50 °C, still dominated by overcharging from excess cations; (c) 20-mer at 10 °C dominated by increased flexibility; (d) 20-mer at 50 °C dominated by thermal motion of the strand; (e) 50-mer at 10 °C dominated by flexibility; and (f) 50-mer at 50 °C, dominated by thermal motion.

lengths. Regardless of strand length, the temperature of maximum current decreases as salt concentration increases, although the range of effects are more pronounced for the 20-mer and 50-mer polyT. This trend demonstrates that the more flexible a strand is initially, the less heat it needs to reach a maximum current/minimum MB-Au distance. The characteristics reflected in Figure 7 are fully consistent with findings in a study that employed fluorescence correlation spectroscopy,[37] which showed that the hydrodynamic radius of polyT decreasing exponentially due to a greater flexibility with increasing salt concentration.

Another interesting set of derived data for the three-strand lengths is shown in Figure 8. The current versus salt concentration results shown are a replotting of results from Figures 4a–6a and selected at two temperatures, 10 °C on the low end and 50 °C on the high end, for each strand length. These "temperature slices" offer an additional confirmation of the phenomenological effects discussed so far. The discussed effects for each case in Figure 8 are depicted with trend arrows, and the hypothesized dominating factor is labeled.

In the case of a 50-mer, the strand is long enough that the MB is generally far away from the Au, yielding low current for low salt concentration and temperature, when d is high. As the salt concentration increases, we again believe that there is significantly increased flexibility in the strand, which brings the MB closer to the WE and raises the current.

A 10-mer strand seems to display an entirely opposite trend. This strand may only require a low salt concentration to increase its flexibility, bringing the MB closer to the Au, thus decreasing d for low [NaCl]. The MB moves farther away in high salt concentrations, increasing d and diminishing the measured current as it becomes more rigid due to overcharging. We see this trend at both 10 and 50 °C for the 10-mer, although the higher temperature yields a lower current, most likely due to the effects of stretching.

The 20-mer strand, which we suggested earlier has two different regimes, appears to behave in a somewhat intermediate manner (as might be expected) between the 10-mer and 50-mer, although its trends are more similar to the 50-mer than the 10-mer. This observation means that salt concentration and temperature must have a more varied overall effect on the position of the MB on medium-length and long strands than for shorter strands, which seem more dominated by a single factor.

CONCLUSIONS

The majority of studies on electrochemical DNA biosensors focus on dsDNA and their melting profiles and hybridization abilities. Here, we have studied a much simple case, using ssDNA of thymines at varying lengths. However, understanding how dsDNA hybridization occurs under varying conditions provides a clearer idea of how ssDNA's conformation might be affected, which in turn is related to its ability to bind to a target analyte. In this study, we used small-volume samples and alternating sequential methods to effectively and quickly complete data acquisition for a set of electrochemical studies of immobilized polyT strands of different lengths at variable salt concentrations and temperatures. Parametric changes and thermal ramps could be investigated on a single device without introducing day-to-day variations. The obtained results serve as a baseline for understanding how external stressors, such as chemical environment and heat, affect the conformation of modified DNA, and therefore, the distance between the moiety and the

https://dx.doi.org/10.1021/acs.langmuir.0c03219
Langmuir 2021, 37, 2607–2618

working electrode of the device. It also provides insights into how these stress factors affect a strand differently depending on its length.

From our results, we see that the effects of salt do, indeed, affect the conformation of the DNA, as expected. However, when introducing temperature variations as well as length variations, the results are not always what might initially be expected. The effects of stretching due to temperature increase seem to decrease the average current for a short, 10-mer strand, which, in low salt, has its methylene blue moiety relatively closer to the Au surface compared to longer strands. We observed what appeared to be overcharging effects for a 10-mer at moderate to high salt concentrations, due to the comparatively minimal amount of charge of the 10-mer, which makes it easily overcharged by working buffer ions. For a 50-mer, the behavior with increased salt concentration is increased flexibility, which brings the MB closer to the WE and increases current. Current increases are also observed due to thermal motion lowering the MB−WE distance a bit further. For a medium-length polyT strand such as a 20-mer, we see behavior that is somewhat intermediate, but more similar to a 50-mer than a 10-mer. Due to the effects of salt and temperature on the motion and conformation of a single strand of DNA, we believe that increased thermal motion as a result of high temperatures and increased flexibility from high salt might actually hinder a ssDNA's ability to bind to a target analyte, although finding the ideal conditions for binding would be unique to the DNA stand and depend on length, sequence, and secondary or tertiary structures.

The results here will be helpful as a foundation for future investigations of how salt and temperature variations affect the conformation of more complex immobilized aptamers, as well as their ability to bind to target, for the purpose of biosensing in medical diagnostic work. This knowledge can be used for sensing DNA in solutions more complex and medically relevant than PBS, such as human serum, urine, or sweat. Future studies may explore the variations of frequency on ssDNA conformation and signal strength in conjunction with varying temperature, strand length, and salt concentration. Additionally, these results are also suitable for computational work, to more quickly assess the effects of additional stressors such as divalent (Mg^{2+}) or trivalent (Al^{3+}, Co^{3+}) cations, increased heat, or deviations in pH.

■ ASSOCIATED CONTENT

Supporting Information

The Supporting Information is available free of charge at https://pubs.acs.org/doi/10.1021/acs.langmuir.0c03219.

It includes XPS data, electrochemical control program and data collection methods, and signal reversibility and reproducibility (PDF)

■ AUTHOR INFORMATION

Corresponding Author

Ramya Vishnubhotla − *Biomolecular Measurement Division, National Institute of Standards and Technology, Gaithersburg, Maryland 20899, United States;* orcid.org/0000-0001-7172-2578; Email: rvi@sas.upenn.edu

Authors

Christopher B. Montgomery − *Biomolecular Measurement Division, National Institute of Standards and Technology, Gaithersburg, Maryland 20899, United States*

Kristen L. Steffens − *Biomolecular Measurement Division, National Institute of Standards and Technology, Gaithersburg, Maryland 20899, United States*

Steve Semancik − *Biomolecular Measurement Division, National Institute of Standards and Technology, Gaithersburg, Maryland 20899, United States*

Complete contact information is available at: https://pubs.acs.org/10.1021/acs.langmuir.0c03219

Author Contributions

R.V. designed and executed the experiments in this work and drafted the manuscript. C.B.M. mounted the electrochemical microdevices used in these studies. K.L.S obtained the XPS data used to characterize the density of the immobilized species on the working electrode. S.S. assisted in the design of the study as well as the preparation of the manuscript.

Notes

The authors declare no competing financial interest.

Commercial equipment and materials are identified to adequately specify certain procedures. In no case does such identification imply recommendation or endorsement by National Institute of Standards and Technology, nor does it imply the materials or equipment identified are necessarily the best available for the purpose.

■ ACKNOWLEDGMENTS

R.V. acknowledges funding from the NIST—National Research Council Research Associateship Program. The authors thank Dr. Sarah Robinson for device fabrication and Dr. Dean Ripple for useful discussions of the experiments and manuscript. The authors also thank Dr. Rebecca Zangmeister, Dr. Sean Lehman, Dr. Kurt Benkstein, Dr. Nicole Ritzert, and Dr. Ryan West for their readings of the manuscript during its preparation. The research was performed, in part, at the NIST Center for Nanoscale Science and Technology.

■ REFERENCES

(1) Liepold, P.; Kratzmüller, T.; Persike, N.; Bandilla, M.; Hinz, M.; Wieder, H.; Hillebrandt, H.; Ferrer, E.; Hartwich, G. Electrically detected displacement assay (EDDA): a practical approach to nucleic acid testing in clinical or medical diagnosis. *Anal. Bioanal. Chem.* **2008**, *391*, 1759−1772.

(2) Sohrabi, N.; Valizadeh, A.; Farkhani, S. M.; Akbarzadeh, A. Basics of DNA biosensors and cancer diagnosis. *Artif. Cells, Nanomed., Biotechnol.* **2016**, *44*, 654−663.

(3) Hassan, R. A.; Heng, L. Y.; Tan, L. L. Novel DNA Biosensor for Direct Determination of Carrageenan. *Sci. Rep.* **2019**, *9*, No. 6379.

(4) Senel, M.; Dervisevic, M.; Kokkokoğlu, F. Electrochemical DNA biosensors for label-free breast cancer gene marker detection. *Anal. Bioanal. Chem,* **2019**, *411*, 2925−2935.

(5) Ping, J.; Vishnubhotla, R.; Vrudhula, A.; Johnson, A. T. C. Scalable Production of High-Sensitivity, Label-Free DNA Biosensors Based on Back-Gated Graphene Field Effect Transistors. *ACS Nano* **2016**, *10*, 8700−8704.

(6) Vishnubhotla, R.; Ping, J.; Gao, Z.; Lee, A.; Saouaf, O.; Vrudhula, A.; Johnson, A. T. C. Scalable graphene aptasensors for drug quantification. *AIP Adv.* **2017**, *7*, No. 115111.

(7) Zouari, M.; Campuzano, S.; Pingarrón, J. M.; Raouafi, N. Amperometric Biosensing of miRNA-21 in Serum and Cancer Cells at

Nanostructured Platforms Using Anti-DNA−RNA Hybrid Antibodies. *ACS Omega* **2018**, *3*, 8923−8931.
(8) Campuzano, S.; Pedrero, M.; Pingarrón, J. M. Viral protein-based bioanalytical tools for small RNA biosensing. *TrAC, Trends Anal. Chem.* **2016**, *79*, 335−343.
(9) Luo, X.; Hsing, I. M. Real Time Electrochemical Monitoring of DNA/PNA Dissociation by Melting Curve Analysis. *Electroanalysis* **2009**, *21*, 1557−1561.
(10) Paleček, E. Changes in oscillopolarographic behaviour of deoxyribonucleic acids at temperatures below denaturation temperature. *J. Mol. Biol.* **1965**, *11*, 839−841.
(11) Kang, D.; Zuo, X.; Yang, R.; Xia, F.; Plaxco, K. W.; White, R. J. Comparing the Properties of Electrochemical-Based DNA Sensors Employing Different Redox Tags. *Anal. Chem.* **2009**, *81*, 9109−9113.
(12) Furst, A.; Hill, M. G.; Barton, J. K. Electrocatalysis in DNA Sensors. *Polyhedron* **2014**, *84*, 150−159.
(13) Li, C.; Hu, X.; Lu, J.; Mao, X.; Xiang, Y.; Shu, Y.; Li, G. Design of DNA Nanostructure-Based Interfacial Probes for the Electrochemical Detection of Nucleic Acids Directly in Whole Blood. *Chem. Sci.* **2018**, *9*, 979−984.
(14) Zhang, S.; Huang; Jingrun, Lu. J.; Liu, M.; Li, Y.; Fang, L.; Huang, H.; Huang; Jianjun, Mo. F.; Zheng, J. A Novel Fluorescent Biosensor Based on Dendritic DNA Nanostructure in Combination with Ligase Reaction for Ultrasensitive Detection of DNA Methylation. *J. Nanobiotechnol.* **2019**, *17*, No. 121.
(15) Shi, S.; Wang, X.; Sun, W.; Wang, X.; Yao, T.; Ji, L. Label-free fluorescent DNA biosensors based on metallointercalators and nanomaterials. *Methods* **2013**, *64*, 305−314.
(16) Pyrak, E.; Krajczewski, J.; Kowalik, A.; Kudelski, A.; Jaworska, A. Surface Enhanced Raman Spectroscopy for DNA Biosensors—How Far Are We? *Molecules* **2019**, *24*, No. 4423.
(17) Drozd, M.; Pietrzak, M. D.; Malinowska, E. SPRi-Based Biosensing Platforms for Detection of Specific DNA Sequences Using Thiolate and Dithiocarbamate Assemblies. *Front. Chem.* **2018**, *6*, 1−12.
(18) Yang, A. H.; Hsieh, K.; Patterson, A. S.; Ferguson, B. S.; Eisenstein, M.; Plaxco, K. W.; Soh, H. T. Accurate zygote-specific discrimination of single-nucleotide polymorphisms using microfluidic electrochemical DNA melting curves. *Angew. Chem., Int. Ed.* **2014**, *53*, 3163−3167.
(19) Robinson, S. M.; Shen, Z.; Askim, J. R.; Montgomery, C. B.; Sintim, H. O.; Semancik, S. Ligand-Based Stability Changes in Duplex DNA Measured with a Microscale Electrochemical Platform. *Biosensors* **2019**, *9*, No. 54.
(20) Rahman, M. M.; Li, X. B.; Lopa, N. S.; Ahn, S. J.; Lee, J. J. Electrochemical DNA hybridization sensors based on conducting polymers. *Sensors* **2015**, *15*, 3801−3829.
(21) Shen, Z.; Sintim, H. O.; Semancik, S. Rapid nucleic acid melting analyses using a microfabricated electrochemical platform. *Anal. Chim. Acta* **2015**, *853*, 265−270.
(22) Kang, D.; Parolo, C.; Sun, S.; Ogden, N. E.; Dahlquist, F. W.; Plaxco, K. W. Expanding the Scope of Protein-Detecting Electrochemical DNA "Scaffold" Sensors. *ACS Sens.* **2018**, *3*, 1271−1275.
(23) Yang, J.; Dou, B.; Yuan, R.; Xiang, Y. Aptamer/Protein Proximity Binding-Triggered Molecular Machine for Amplified Electrochemical Sensing of Thrombin. *Anal. Chem.* **2017**, *89*, 5138−5143.
(24) Baker, B. R.; Lai, R. Y.; Wood, M. S.; Doctor, E. H.; Heeger, A. J.; Plaxco, K. W. An Electronic, Aptamer-Based Small-Molecule Sensor for the Rapid, Label-Free Detection of Cocaine in Adulterated Samples and Biological Fluids. *J. Am. Chem. Soc.* **2006**, *128*, 3138−3139.
(25) Hayat, A.; Marty, J. L. Aptamer based electrochemical sensors for emerging environmental pollutants. *Front. Chem.* **2014**, *2*, 1−9.
(26) Li, F.; Yu, Z.; Han, X.; Lai, R. Y. Electrochemical aptamer-based sensors for food and water analysis: A review. *Anal. Chim. Acta* **2019**, *1051*, 1−23.
(27) D'Agata, R.; Giuffrida, M. C.; Spoto, G. Peptide Nucleic Acid-Based Biosensors for Cancer Diagnosis. *Molecules* **2017**, *22*, No. 1951.
(28) Wang, W.; Chen, C.; Qian, M. X.; Zhao, X. S. Aptamer biosensor for protein detection based on guanine-quenching. *Sens. Actuators, B* **2008**, *129*, 211−217.
(29) Murphy, M. C.; Rasnik, I.; Cheng, W.; Lohman, T. M.; Ha, T. Probing single-stranded DNA conformational flexibility using fluorescence spectroscopy. *Biophys. J.* **2004**, *86*, 2530−2537.
(30) Park, N.; Hahn, J. H. Electrochemical Sensing of DNA Hybridization Based on Duplex-Specific Charge Compensation. *Anal. Chem.* **2004**, *76*, 900−906.
(31) Li, C.; Li, X.; Wei, L.; Liu, M.; Chen, Y.; Li, G. Simple Electrochemical Sensing of Attomolar Proteins Using Fabricated Complexes with Enhanced Surface Binding Avidity. *Chem. Sci.* **2015**, *6*, 4311−4317.
(32) Surkus, A.-E.; Flechsig, G.-U. Electrochemical Detection of DNA Melting Curves by Means of Heated Biosensors. *Electroanalysis* **2009**, *21*, 1119−1123.
(33) Nasef, H.; Beni, V.; O'Sullivan, C. K. Electrochemical melting-curve analysis. *Electrochem. Commun.* **2010**, *12*, 1030−1033.
(34) Nasef, H.; Beni, V.; O'Sullivan, C. K. Labelless electrochemical melting curve analysis for rapid mutation detection. *Anal. Methods* **2010**, *2*, 1461−1466.
(35) Nasef, H.; Ozalp, V. C.; Beni, V.; O'Sullivan, C. K. Melting temperature of surface-tethered DNA. *Anal. Biochem.* **2010**, *406*, 34−40.
(36) Biala, K.; Sedova, A.; Flechsig, G. U. Sequence and Temperature Influence on Kinetics of DNA Strand Displacement at Gold Electrode Surfaces. *ACS Appl. Mater. Interfaces* **2015**, *7*, 19948−19959.
(37) Doose, S.; Barsch, H.; Sauer, M. Polymer Properties of Polythymine as Revealed by Translational Diffusion. *Biophys. J.* **2007**, *93*, 1224−1234.
(38) Silva, S. M.; Tavallaie, R.; Gonçales, V. R.; Utama, R. H.; Kashi, M. B.; Hibbert, D. B.; Tilley, R. D.; Gooding, J. J. Dual Signaling DNA Electrochemistry: An Approach To Understand DNA Interfaces. *Langmuir* **2018**, *34*, 1249−1255.
(39) Uzawa, T.; Cheng, R. R.; White, R. J.; Makarov, D. E.; Plaxco, K. W. A Mechanistic Study of Electron Transfer from the Distal Termini of Electrode-Bound, Single-Stranded DNAs. *J. Am. Chem. Soc.* **2010**, *132*, 16120−16126.
(40) Anne, A.; Bouchardon, A.; Moiroux, J. 3'-Ferrocene-Labeled Oligonucleotide Chains End-Tethered to Gold Electrode Surfaces: Novel Model Systems for Exploring Flexibility of Short DNA Using Cyclic Voltammetry. *J. Am. Chem. Soc.* **2003**, *125*, 1112−1113.
(41) Contento, N. M.; Semancik, S. Thermal characteristics of temperature-controlled electrochemical microdevices. *Sens. Actuators, B* **2016**, *225*, 279−287.
(42) White, R. J.; Plaxco, K. W. In *Engineering New Aptamer Geometries for Electrochemical Aptamer-Based Sensors*, Bio-Inspired/Biomimetic Sensor Technologies and Applications, 2009; 732105.
(43) Gooding, J. J. Electrochemical DNA Hybridization Biosensors. *Electroanalysis* **2002**, *14*, 1149−1156.
(44) Movilli, J.; Rozzi, A.; Ricciardi, R.; Corradini, R.; Huskens, J. Control of Probe Density at DNA Biosensor Surfaces Using Poly(l-lysine) with Appended Reactive Groups. *Bioconjugate Chem.* **2018**, *29*, 4110−4118.
(45) Murphy, J. N.; Cheng, A. K. H.; Yu, H.-Z.; Bizzotto, D. On the Nature of DNA Self-Assembled Monolayers on Au: Measuring Surface Heterogeneity with Electrochemical in Situ Fluorescence Microscopy. *J. Am. Chem. Soc.* **2009**, *131*, 4042−4050.
(46) Bizzotto, D.; Burgess, I. J.; Doneux, T.; Sagara, T.; Yu, H.-Z. Beyond Simple Cartoons: Challenges in Characterizing Electrochemical Biosensor Interfaces. *ACS Sens.* **2018**, *3*, 5−12.
(47) Rashid, J. I. A.; Yusof, N. A. The strategies of DNA immobilization and hybridization detection mechanism in the construction of electrochemical DNA sensor: A review. *Sens. Bio-Sens. Res.* **2017**, *16*, 19−31.
(48) Farjami, E.; Clima, L.; Gothelf, K.; Ferapontova, E. E. "Off−On" Electrochemical Hairpin-DNA-Based Genosensor for Cancer Diagnostics. *Anal. Chem.* **2011**, *83*, 1594−1602.

https://dx.doi.org/10.1021/acs.langmuir.0c03219
Langmuir 2021, 37, 2607−2618

(49) Wu, Y.; Lai, R. Y. Tunable Signal-Off and Signal-On Electrochemical Cisplatin Sensor. *Anal. Chem.* **2017**, *89*, 9984−9989.
(50) Ma, R.; Wang, L.; Zhang, M.; Jia, L.; Zhang, W.; Shang, L.; Jia, W.; Wang, H. A Novel One-Step Triggered "Signal-On/Off" Electrochemical Sensing Platform for Lead Based on the Dual-Signal Ratiometric Output and Electrode-Bound DNAzyme Assembly. *Sens. Actuators, B* **2018**, *257*, 678−684.
(51) Silva, S. M.; Hoque, S.; Gonçales, V. R.; Gooding, J. J. The Impact of the Position of the Redox Label on Charge Transfer and Hybridization Efficiency at DNA Interfaces. *Electroanalysis* **2018**, *30*, 1529−1535.
(52) Pumera, M.; Ambrosi, A.; Bonanni, A.; Chng, E. L. K.; Poh, H. L. Graphene for electrochemical sensing and biosensing. *TrAC, Trends Anal. Chem.* **2010**, *29*, 954−965.
(53) Tu, J.; Gan, Y.; Liang, T.; Hu, Q.; Wang, Q.; Ren, T.; Sun, Q.; Wan, H.; Wang, P. Graphene FET Array Biosensor Based on ssDNA Aptamer for Ultrasensitive Hg2+ Detection in Environmental Pollutants. *Front. Chem.* **2018**, *6*, 1−9.
(54) Shao, Y.; Wang, J.; Wu, H.; Liu, J.; Aksay, I. A.; Lin, Y. Graphene Based Electrochemical Sensors and Biosensors: A Review. *Electroanalysis* **2010**, *22*, 1027−1036.
(55) Seidel, C. A. M.; Schulz, A.; Sauer, M. H. M. Nucleobase-Specific Quenching of Fluorescent Dyes. 1. Nucleobase One-Electron Redox Potentials and Their Correlation with Static and Dynamic Quenching Efficiencies. *J. Phys. Chem. A* **1996**, *100*, 5541−5553.
(56) Pheeney, C. G.; Barton, J. K. DNA Electrochemistry with Tethered Methylene Blue. *Langmuir* **2012**, *28*, 7063−7070.
(57) Ramaley, L.; Krause, M. S. Theory of square wave voltammetry. *Anal. Chem.* **1969**, *41*, 1362−1365.
(58) Turner, J. A.; Christie, J. H.; Vukovic, M.; Osteryoung, R. A. Square wave voltammetry at the dropping mercury electrode: experimental. *Anal. Chem.* **1977**, *49*, 1904−1908.
(59) Meunier-Prest, R.; Raveau, S.; Finot, E.; Legay, G.; Cherkaoui-Malki, M.; Latruffe, N. Direct measurement of the melting temperature of supported DNA by electrochemical method. *Nucleic Acids Res.* **2003**, *31*, No. e150.
(60) Kaiser, W.; Rant, U. Conformations of End-Tethered DNA Molecules on Gold Surfaces: Influences of Applied Electric Potential, Electrolyte Screening, and Temperature. *J. Am. Chem. Soc.* **2010**, *132*, 7935−7945.
(61) Sosnowski, R. G.; Tu, E.; Butler, W. F.; O'Connell, J. P.; Heller, M. J. Rapid determination of single base mismatch mutations in DNA hybrids by direct electric field control. *Proc. Natl. Acad. Sci. U.S.A.* **1997**, *94*, 1119−1123.
(62) Siebert, T.; Guchhait, B.; Liu, Y.; Fingerhut, B. P.; Elsaesser, T. Range, Magnitude, and Ultrafast Dynamics of Electric Fields at the Hydrated DNA Surface. *J. Phys. Chem. Lett.* **2016**, *7*, 3131−3136.
(63) Rant, U.; Arinaga, K.; Tornow, M.; Kim, Y. W.; Netz, R. R.; Fujita, S.; Yokoyama, N.; Abstreiter, G. Dissimilar Kinetic Behavior of Electrically Manipulated Single- and Double-Stranded DNA Tethered to a Gold Surface. *Biophys. J.* **2006**, *90*, 3666−3671.
(64) Anne, A.; Demaille, C. Electron Transport by Molecular Motion of redox-DNA Strands: Unexpectedly Slow Rotational Dynamics of 20-mer ds-DNA Chains End-Grafted onto Surfaces via C6 Linkers. *J. Am. Chem. Soc.* **2008**, *130*, 9812−9823.
(65) Watkins, H. M.; Ricci, F.; Plaxco, K. W. Experimental Measurement of Surface Charge Effects on the Stability of a Surface-Bound Biopolymer. *Langmuir* **2018**, *34*, 14993−14999.
(66) Belkin, M.; Maffeo, C.; Wells, D. B.; Aksimentiev, A. Stretching and Controlled Motion of Single-Stranded DNA in Locally Heated Solid-State Nanopores. *ACS Nano* **2013**, *7*, 6816−6824.
(67) Sim, A. Y. L.; Lipfert, J.; Herschlag, D.; Doniach, S. Salt Dependence of the Radius of Gyration and Flexibility of Single-Stranded DNA in Solution Probed by Small-Angle X-ray Scattering. *Phys. Rev. E* **2012**, *86*, No. 021901.
(68) Batchelor-McAuley, C.; Wildgoose, G. G.; Compton, R. G. The physicochemical aspects of DNA sensing using electrochemical methods. *Biosens. Bioelectron.* **2009**, *24*, 3183−3190.
(69) Guerrero-García, G. I.; González-Tovar, E.; Chávez-Páez, M.; Lozada-Cassou, M. Overcharging and charge reversal in the electrical double layer around the point of zero charge. *J. Chem. Phys.* **2010**, *132*, No. 054903.
(70) Deserno, M.; Jiménez-Ángeles, F.; Holm, C.; Lozada-Cassou, M. Overcharging of DNA in the Presence of Salt: Theory and Simulation. *J. Phys. Chem. B* **2001**, *105*, 10983−10991.
(71) Wenner, J. R.; Williams, M. C.; Rouzina, I.; Bloomfield, V. A. Salt dependence of the elasticity and overstretching transition of single DNA molecules. *Biophys. J.* **2002**, *82*, 3160−3169.

https://dx.doi.org/10.1021/acs.langmuir.0c03219
Langmuir 2021, 37, 2607−2618